INVESTIGATION OF TITANIUM ALLOYS UNDER BIAXIAL IMPACT LOADING

Final Technical Report

by

Prof. Dr.-Ing. L. W. Meyer
Dipl.-Ing. L. Krueger

United States Army

EUROPEAN RESEARCH OFFICE OF THE U. S. ARMY

London England

CONTRACT NUMBER C-N68171-96-C-9095

Nordmetall GbR

Approved for Public Release; distribution unlimited

19970910 113

REPORT DOCUMENTATION PAGE

Public reporting burden for this collection of information is estimated to average 1 hour per response, including the time for reviewing instructions, searching existing data sources, gathering and maintaining the data needed, and completing and reviewing the collection of information. Send comments regarding this burden estimate or any other aspect of this collection of information, including suggestions for reducing this burden to Washington Headquarters Services, Directorate for Information Operations and Reports, 1215 Jefferson Davis Highway, Suite 1204, Arlington, VA 22202-4302, and to the Office of Management and Budget, Paperwork Reduction Project (0704-0188), Washington, DC 20503.

1. AGENCY USE ONLY (Leave blank)	2. REPORT DATE 07 July 1997	3. REPORT TYPE AND DATES COVERED Final Technical Report 25 Aug 96 - 07. July 97

4. TITLE AND SUBTITLE Investigation of Titanium Alloys under Biaxial Impact Loading	5. FUNDING NUMBERS C-N68171-96-C-9095

6. AUTHOR(S) Lothar W. Meyer Lutz Krueger	

7. PERFORMING ORGANIZATION NAME(S) AND ADDRESS(ES) NORDMETALL GbR Bergstr. 1 Ge-09366 STOLLBERG, Germany	8. PERFORMING ORGANIZATION REPORT NUMBER NMB-2

9. SPONSORING/MONITORING AGENCY NAME(S) AND ADDRESS(ES) TU Chemnitz-Zwickau Chemnitz, Germany	10. SPONSORING/MONITORING AGENCY REPORT NUMBER

11. SUPPLEMENTARY NOTES

12a. DISTRIBUTION/AVAILABILITY STATEMENT	12b. DISTRIBUTION CODE

13. ABSTRACT (Maximum 200 words)

Ti-6Al-4V titanium alloy was subjected to three heat treatment conditions. Ballistic tests at ARL have shown differences in the ballistic performance, if annealed above the beta transus temperature. Mechanical tests under uniaxial compression as well as biaxial compression/shear-stress states and high strain rates in the range of 10^2 s^{-1} were performed at TU Chemnitz. Additionally, quasistatic compression tests were performed. Scanning electron microscopy was used to correlate deformation structures of shear cracks from ballistic tests with that of laboratory shear specimens. Indications of interdependencies between the ballistic performance and mechanical behavior under compression/shear loading of different heat treated titanium targets were noted, e. g. dynamic strength and sensitivity to adiabatic shear failure.

DTIC QUALITY INSPECTED 4

14. SUBJECT TERMS failure mechanism at high strain rates; biaxial loading; titanium alloy			15. NUMBER OF PAGES 28
			16. PRICE CODE

17. SECURITY CLASSIFICATION OF REPORT UL	18. SECURITY CLASSIFICATION OF THIS PAGE UL	19. SECURITY CLASSIFICATION OF ABSTRACT UL	20. LIMITATION OF ABSTRACT UL

INVESTIGATION OF TITANIUM ALLOYS

UNDER

BIAXIAL IMPACT LOADING

ABSTRACT:

Mechanical and ballistic tests were performed on Ti-6Al-4V titanium alloy subjected to three heat treatment conditions. Ballistic performance were analyzed at ARL. For the samples annealed above the beta transus temperature, a loss in ballistic performance was noted and the samples exhibited little bulk deformation and bulging, but extensive adiabatic shear banding. Samples annealed below the beta transus temperature exhibited extensive bulk deformation and rear surface bulging, delaminations perpendicular to the penetrator path with shear bands parallel to the direction of impact.

In mechanical tests, dynamic strength and failure behaviour of Ti-6Al-4V under compression and biaxial compression/shear loading has been investigated at TU Chemnitz. Scanning electron microscopy (SEM) was used to correlate deformation structures of shear cracks from ballistic tests with that of laboratory shear specimens. Similar fracture behaviour was found in both sheared compression/shear and ballistic samples. Indications of an relationship between the ballistic performance and mechanical behaviour under compression/shear loading of different heat treated titanium targets were noted, e.g. dynamic strength and sensitivity to adiabatic shear failure.

TABLE OF CONTENTS

LIST OF FIGURES

LIST OF TABLES

1   INTRODUCTION

Based on the chemical composition, titanium alloys consist of different crystallographic modification. Dependent on their microstructure, each alloy family serves a specific role. For instance, titanium alloys are excellent candidates for aircraft applications owing to their high strength to weight ratio and corrosion resistance [1]. However, the relatively high cost of titanium coupled with the limited information on its ballistic properties have prevented widespread use of titanium as a protective material for application to ground vehicles.

The potential use of titanium for ballistic applications has accelerated recently with the development of low-cost alloys as well as the ballistic evaluation and development of penetration algorithms for titanium against modern long-rod penetrators [2, 3, 4]. The ballistic advantages of titanium targets against these rods was about 60% higher than reference ballistic steel and can be attributed to the lower density combined with uniform hardness and equal or greater strength over similar thick cross-sections of steel. Evident in the penetration channels of these semi-infinite titanium blocks was extensive radial adiabatic shear banding from the high-strain rate impacts [5, 6]. The effect of shear banding during deep semi-infinite penetration is not understood, but significantly effects the breakout phase during perforation of finite plates.

Because of the importance of adiabatic shear phenomena in military and civil applications, numerous investigations have been performed under laboratory [8, 9, 10, 11, 12, 13] as well as numerical conditions [14 ,15].

Most of the laboratory experiments to study the susceptibility to adiabatic shear failure were performed under pure shear loads in dynamic torsion tests [8, 9] or by using special shear specimen [10, 11]. However, in most impact events biaxial as well as triaxial stress-state conditions may occur. The investigation of the material behaviour under this stress-state condition is still in progress. Therefore, a program was started in order to measure mechanical strength and failure properties under combined compression / shear loading.

Ti-6Al-4V alloys with the same chemical composition but different heat treatment condition were selected, showing differences in their ballistic performance.

The aim of this research was to find indications for interdependencies between ballistic performance of the different heat treated titanium alloys and their material behaviour under high strain rates. Analysis and extensive investigation of the mechanical strength and failure behaviour of three titanium samples taken from the previously tested ballistic plates and subjected to different strain rates under compression were performed. Dynamic biaxial compression-shear experiments were also carried out in order to differentiate the propensity to adiabatic shear failure. Metallographic as well as fractographic investigations were performed on both, sheared and fractured laboratory and ballistic samples.

2   MATERIALS AND TESTING METHODS

2.1   MATERIALS

The titanium specimens used in these tests were standard Ti-6Al-4V, the most common titanium alloy. This material contains mixtures of α and β phases and is classified as an α-β-alloy. For this investigations, extra-low interstitial (ELI) grade titanium produced by RMI Titanium Company, Niles, Ohio, USA was used. Table 1 summarises the chemical composition.

Table 1: Chemical composition of Ti-6Al-4V ELI, Weight Percent

Al	V	C	O	N	H	Fe	Ti
6,12	4,02	0,01	0,12	0,008	0,0058	0,19	Balance

Starting from a single Ti-6Al-4V ELI grade plate, RMI produced a large 28,5 mm thick plate by 1:1 cross rolling at temperatures below the beta transus temperature (approximately 996 °C). A vacuum creep flatten (VCF) treatment was then performed to flatten and stress relieve the plate. This cycle took approximately 24 hours, including heat-up and cool-down time and reached a temperature of 788 °C. The plate was then cut into ballistic and mechanical test plates. Most of the samples received additional annealing heat treatments. The microstructure of these samples were strongly influenced by the processing history and different heat treatment conditions, [16].

Processing conditions and information about microstructure are found in Table 2. The grain sizes were determined according to the line sectioning method. The microstructure were typical when annealed at the various conditions. Ballistic and mechanical tests were performed on these same materials.

Table 2: Summary of microstructural data for Ti-6Al-4V ELI plates in various annealed conditions

VCF ... vacuum creep flatten treatment, AC ... air cooling

heat treatment condition	characterized microstructure	grain size
VCF only, no anneal	partially recrystallized alpha phase plus intergranular beta phase	α-grains: 16 µm β-grains: 4 µm
899 °C-30 min-AC	predominantly equiaxed alpha phase with increasing amounts of beta phase	α-grains:12,5µm β-grains: 4 µm
1038 °C-30 min-AC	coarse prior beta grains which have transformed to a Widmannstätten alpha-beta microstructure	220 µm

Hardness measurements were performed in each direction of the received plates, Table 3. The fine grained microstructures of condition 67 190 and 67 186 have a similar hardness of about 290 HV 10. The coarse grain material (67 184) is slightly harder when measured in rolling direction of the plate. Microhardness measurements in the bright grain boundaries and in the grains of the coarse grained microstructure have shown small differences in their hardness, Table 4.

2.2 TEST METHODS

The exact main stress state in the impact area and its history is not very well known. Nevertheless, it is assumed, that in the first part of penetration, compression and shear/compression stress states govern the procedure. Therefore, the material behaviour was characterized under both these loading states.

Additionally compression tests were performed on a servohydraulic tension/compression test machine at a strain rate of $\dot{\varepsilon} = 10^{-3}$ s^{-1} and 1 s^{-1}. High strain rate experiments were carried out with drop weight tower at a strain rate of $\dot{\varepsilon} = 200$ s^{-1}. The testing system consists essentially of a heavy drop weight hammer, an anvil and a machine frame, Figure 1. The hammer is guided by a special ball-bearing system in order to ensure a precise alignment of the hammer. The frame and all other parts of the test set-up are of high stiffness to limit elastic deformation. Below the hammer a small punch is fixed to give a precise loading condition as well as to measure the load time history by calibrated strain gauges. The force was measured with calibrated strain gauges and the deformation of the specimens was determined with an opto-electrical system. The force/time and displacement/time signal were registered and stored in a transient recorder, [17]. Adjustable rigid stopping devices make it possible to arrest the impact test at any given point of deformation. Additional details of the experimental procedure have been reported in [18].

A...frame
B...falling weigth
C...tup with force measurement
D...anvil
E...specimen
F...stopping devices
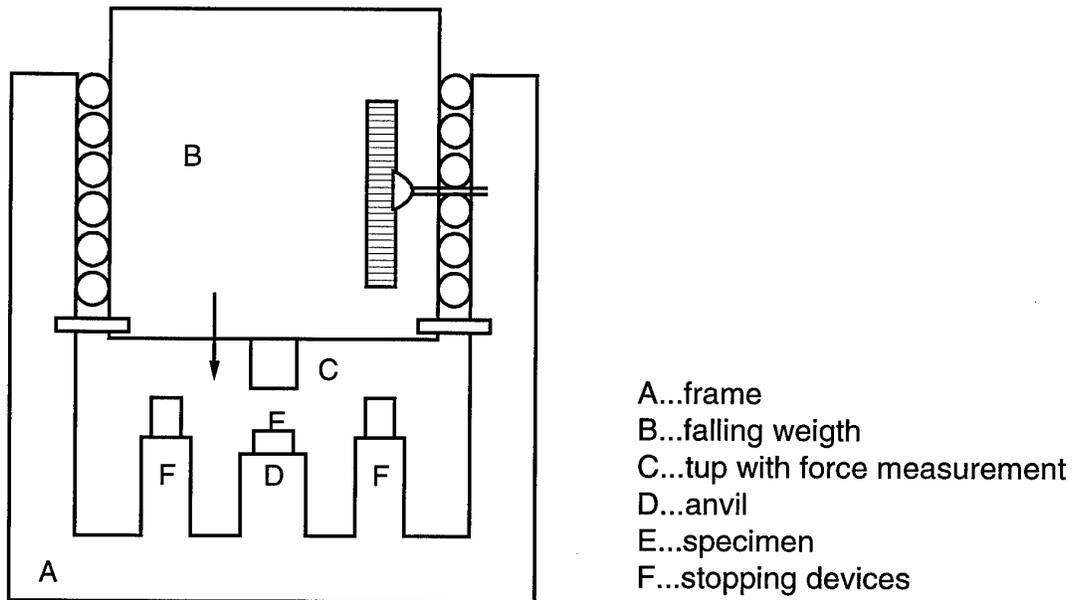
Figure 1: Schematic representation of the drop-weight test set up
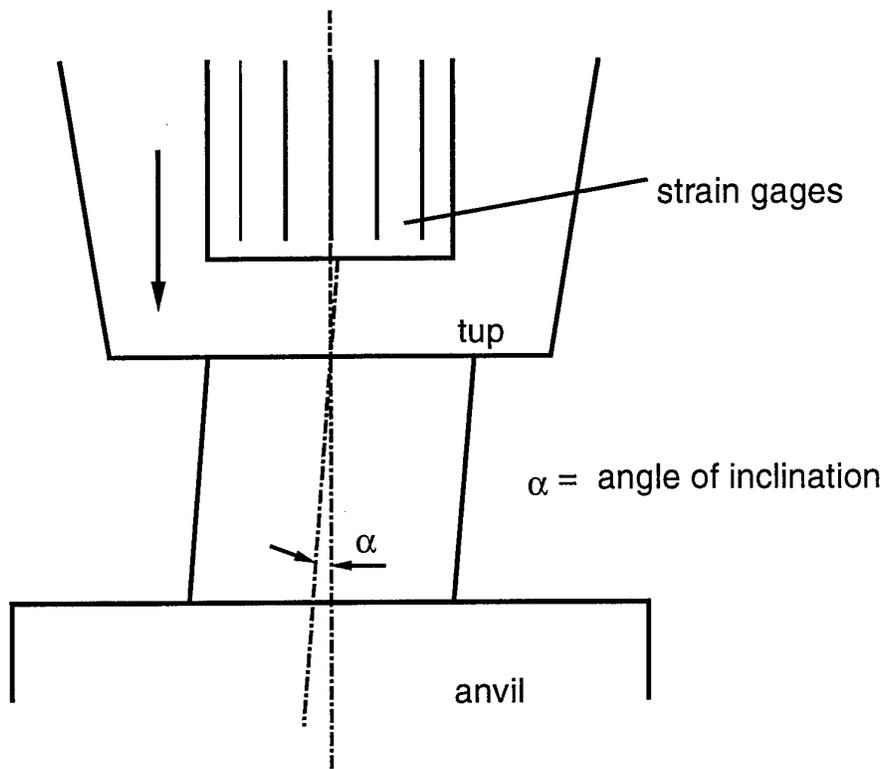
Figure 2: Detail of specimen loading

Specimens for mechanical testing have been machined in thickness direction of the plate. The size of cylindrical compression specimen was 6 mm in diameter and 6 mm in length. To reach a combined compression/shear loading stress state, cylindrical specimens with different inclination angles were tested, Figure 2. Using relatively small inclination of 3 °, 6 ° and 10 °, nearly the same compressive stress distribution is reached as in the non inclined compression specimens. However, this inclination applies additional shear stresses, for example, an inclination angle of 3 ° gives an additional shear loading of 5,2 % of the compression loading acting and an inclination angle of 10 ° yields an additional shear loading of 17,6 % of the axial compression load.

2.3   METALLOGRAPHIC AND FRACTOGRAPHIC EXAMINATIONS

The crater as well as laboratory half-sections were grounded and polished. Final surface etching to reveal the microstructural features was accomplished with a solution composed of 100 ml H_2O, 6 ml HCl, 2 ml H_3PO_4 and 12 ml HF. Etching times were adjusted as necessary for each specimen.
Metallographic and fractographic examinations were taken on both, post mortem ballistic and laboratory samples.
The entire crater wall and near wall region were observed in the light microscope.
Shear band widths were measured in ballistic and laboratory samples. Scanning electron microscopy (SEM) was used in order to investigate the sheared and fractured surfaces.
Additionally, microhardness measurement were performed.

9

3 RESULTS AND DISCUSSION

Dynamic stress-strain curves up to final fracture were obtained for all heat treated conditions up to the strain rate of $\dot{\varepsilon} = 200$ s^{-1}. Microfracture mechanisms were investigated using detailed scanning electron micrographs. Metallographic and fractographic appearance of the failure surfaces of both, penetration crater and tested specimens, were also compared.

3.1 MECHANICAL TESTS

3.1.1 Material behaviour under compression loading

In general, under quasi-static loading at room temperature the material failed at about 30 % compressive deformation for the coarse material and about at 38 % to 45 % for the fine grained microstructures with a nearly homogeneous distributed deformation around the 45 ° shear plane. At strain rates of $\dot{\varepsilon} = 1$ s^{-1} a slightly higher deformability was noticed. At strain rates of about $\dot{\varepsilon} > 100$ s^{-1} the deformability was limited by adiabatic shear failure. Typical stress-strain curves at $\dot{\varepsilon} = 200$ s^{-1} are shown in Figure 3.

The dynamic stress-strain behaviour at strain rates of about $\dot{\varepsilon} = 200$ s^{-1} reaches a maximum compression stress, followed by a rapid drop at fracture. The deformability is limited by adiabatic shear failure.

Typical stress-strain curves at strain rates of about 200 s^{-1}, different heat treatment conditions
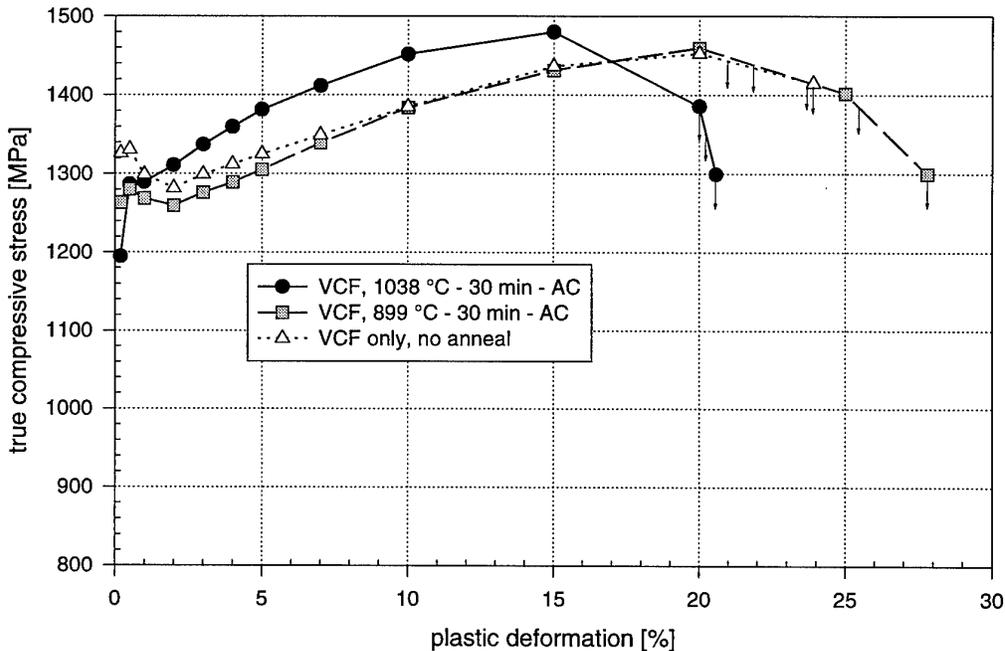
Figure 3: Typical stress-strain curves at strain rates of about $\dot{\varepsilon} = 200$ s^{-1}, different heat treatment conditions

Under dynamic loading condition VCF, no anneal (67190) show a pronounced upper and lower yield point. The other heat treatment conditions have similar 0,2 %-proof stresses, but the coarsed grain material is more strengthen.

Under dynamic uniaxial loading, the coarsed grain material reaches its maximum in strength at lower deformation (about 15 %) than the other material conditions (about 20 %). Additionally, the flow stresses up to 15 % plastic deformation are higher.

The strain-rate dependence of the 0,2%-yield stress is shown in Figure 4. The high strain rate sensitivity is consistent with previous works and results measured by other investigators [19, 20].

Figure numbers on chart legend:
- ● 67 184 (VCF, 1038 °C - 30 min - AC)
- ○ 67 186 (VCF, 899 °C - 30 min - AC)
- ◉ 67 190 (VCF only, no anneal)

y-axis: compression yield strength $\sigma_{0,2}$ [MPa]
x-axis: plastic strain rate [s^{-1}]
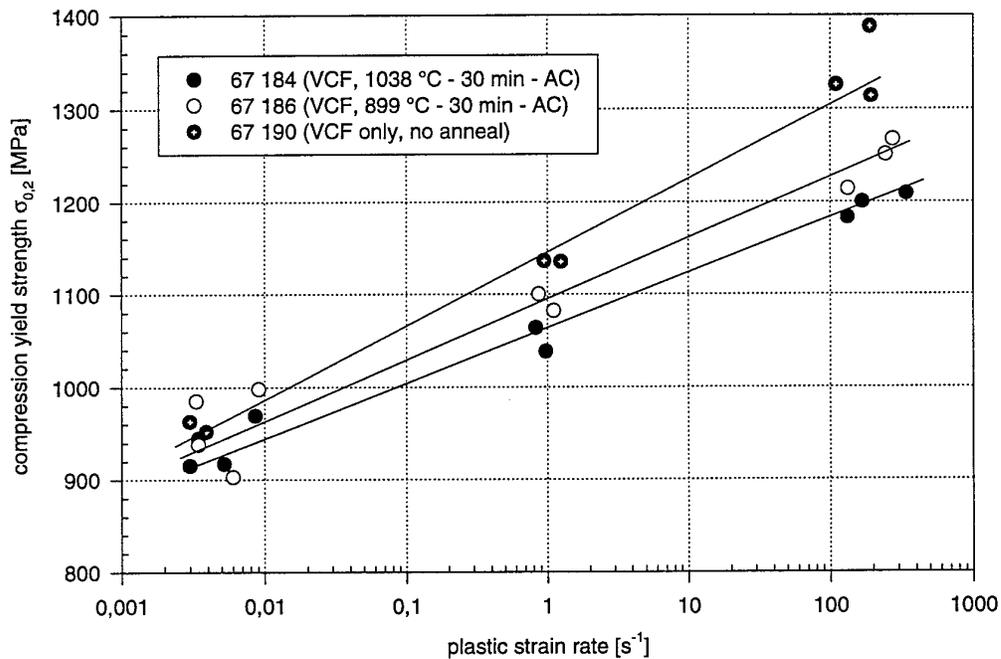
Figure 4: 0,2%-yield strength under compressive loading versus strain rate

From strength and failure behaviour under uniaxial quasistatic and dynamic compression loading, we are able to conclude that there are differences in the ballistic performance of the heat treatment conditions. The ballistic worst coarse grained material shows the lowest deformability under quasi-static as well as dynamic conditions.

Under dynamic loading at strain rates of about $\dot{\varepsilon} \approx 200$ s^{-1}, the coarse material has the highest strength, but on the other hand, it shows the worst deformability compared with the fine grained microstructures.

3.1.2 Material behaviour under dynamic biaxial compression/shear loading

In order to measure the influence of the rolling direction of the plates to adiabatic shear failure inclined specimens with 6 ° inclination in rolling direction as well as crosswise to rolling direction were taken. As a result heat treatment conditions with fine grained microstructures show a pronounced sensitivity to shear if tested in rolling direction of the plate, Figure 5. Hence, all other specimens tested in this program were taken in rolling direction.
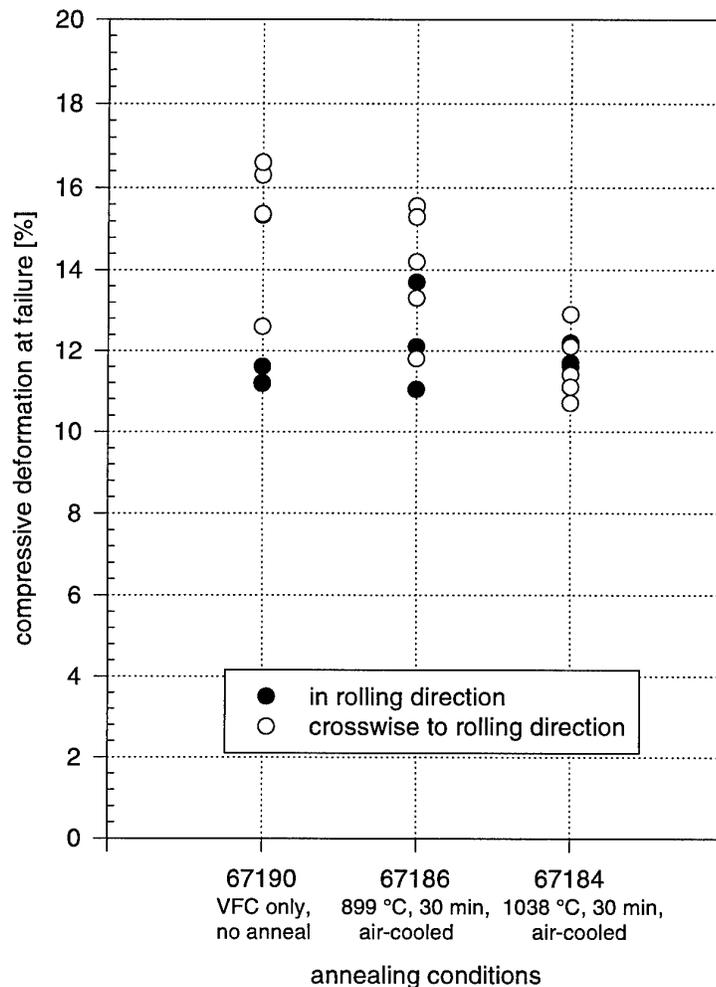
Figure 5: Comparison of compressive deformation of inclined specimens ; shear plane in rolling direction and crosswise to rolling direction, specimen inclination 6°, $\tau/\sigma = 10{,}5$ %   (6grd_efa.spw)

The values of compressive strength and compressive deformation at shear failure as a function of shear/compressive load ratio are given in Figure 6 to Figure 8.
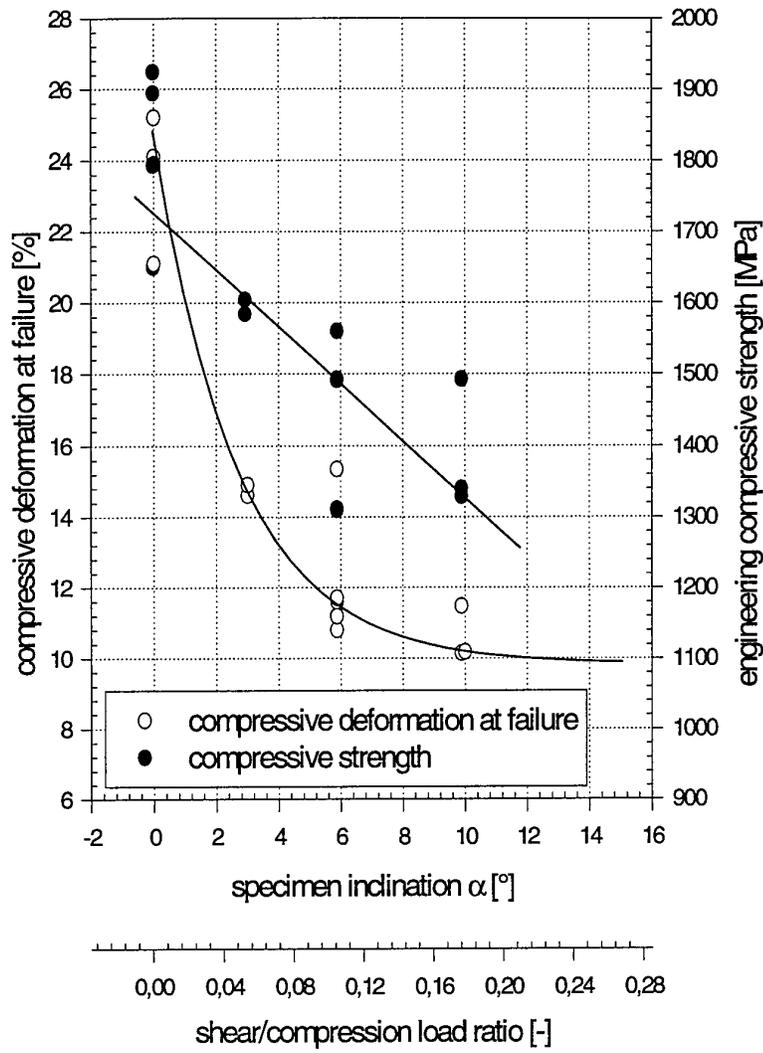
Figure 6: Compressive deformation and compressive strength versus biaxial shear/compression load ratio for 67 190 (VCF, no anneal), (190_modi.spw)
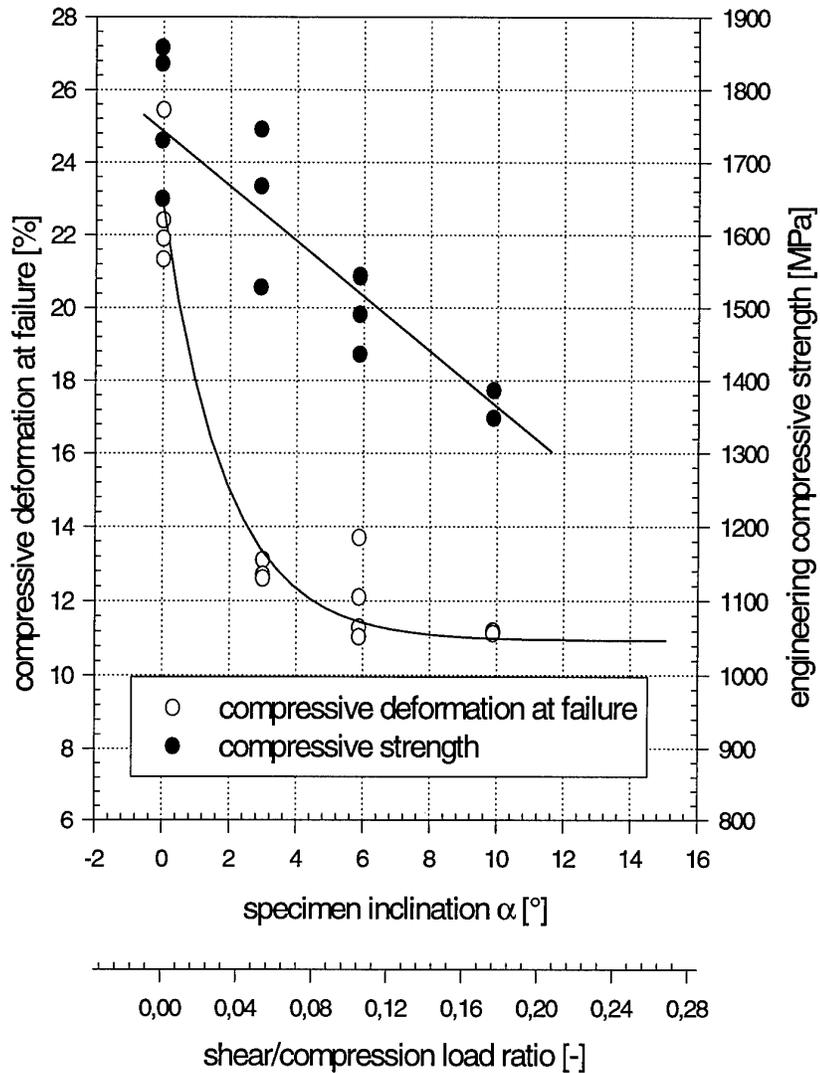
Figure 7: Compressive deformation and compressive strength versus biaxial shear/compression load ratio for 67 186 (VCF and 899 °C-30 min-AC), (186_modi.spw)

An increase in the inclination of the specimen, i.e. the ratio of shear/compression stress leads to a strong reduction of deformability and a reduction of the engineering compressive strength. With increasing shear to compression ratio the adiabatic shear failure occurred at lower strains and lower loads.

Figure 8: Compressive deformation and compressive strength versus biaxial shear/compression load ratio for 67 184 (VCF and 1038 °C-30 min-AC), (184_modi.spw)
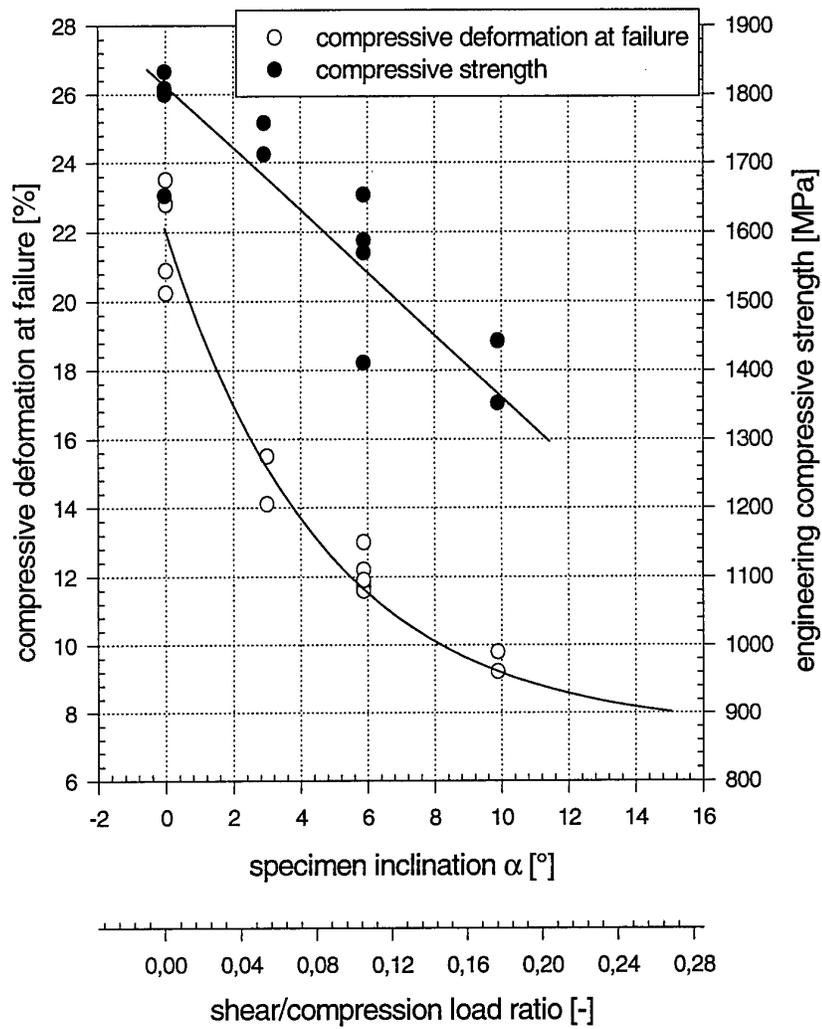
3.2 METALLOGRAPHIC AND FRACTOGRAPHIC EXAMINATION

The ballistic craters as well as the sheared compression/shear specimens were investigated using both, optical microscopy and scanning electron microscopy (SEM). Microstructure of the shear bands was observed by optical microscopy after polishing and etching. The specimens were investigated for microstructural defects, such as microcracks and voids within the shear bands. SEM was employed to observe the surface appearance of the fractured shear surface.

3.2.1 Metallographic examinations

Evaluation of the ballistic craters for the two heat treatment conditions, VCF - not annealed (67 190) and annealed at 899 °C (67 186), show similar failure modes, Figure 9 and Figure 10. A series of parallel shear cracks are formed in the plane of the plate which link together in the direction of the projectile to cause significant deformation, bulging and cracking at the back surface. These separations appear to follow the elongated texture of the alpha-beta rolled and annealed structure.
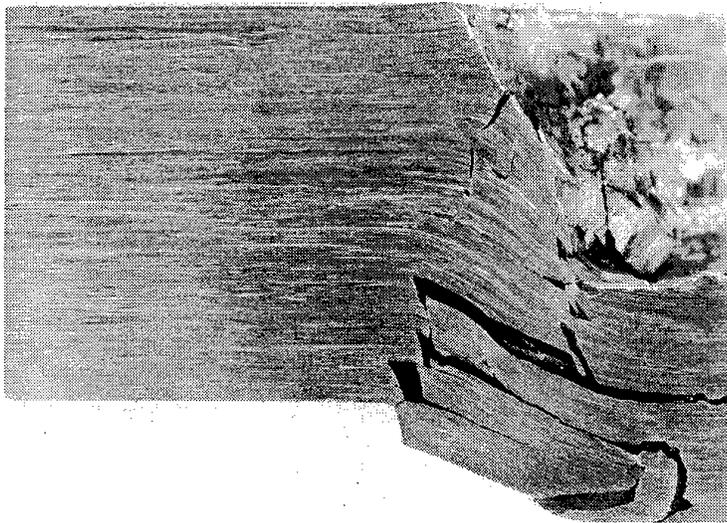
Figure 9: Ballistic crater of 67 190, VCF, no anneal, Magnification: 2x
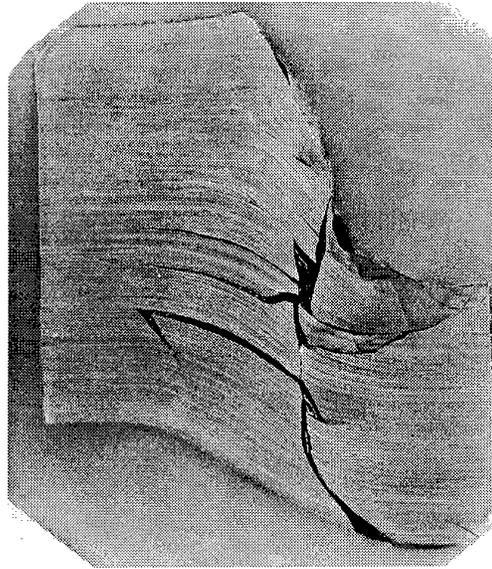
Figure 10: Ballistic crater of 67 186, VCF and 899 °C-30 min-AC, Magnification: 2x

In comparison with the previous conditions, deformation and fracture characteristics of the beta annealed condition (1038 °C) are different, Figure 11. Multiple shear cracks in layers were not evident. Instead, a fewer number of vertical or 45 ° cracks were present. The material tends to plug out but not to spall.
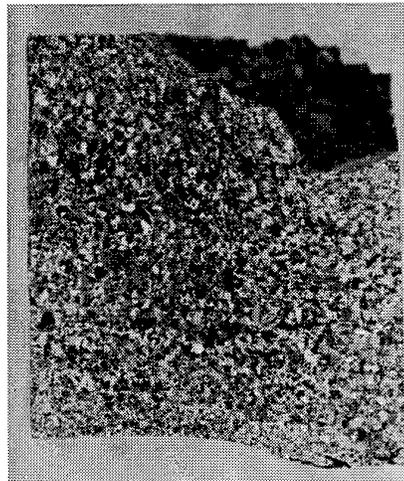
Figure 11: Ballistic crater of 67 184, VCF and 1038 °C-30 min-AC, Magnification: 2x

Figure 12 shows an example of an adiabatic shear band in the ballistic crater of the coarse grained material.

**Figure 12: Adiabatic shear band as a precursor for voids and cracks. Ballistic sample.
VCF, 1038 °C-30 min-AC, Magnification: 50x**

In all three microstructures tested under mechanical high strain rates and ballistic conditions, fracture always proceeds through the growth and coalescence of voids and cracks along the shear bands. Both, elongated ductile dimples and smoothed surface area are typical on most of the fracture surfaces of compression/shear and ballistic samples.

3.2.2 Fractographic examinations

Melting has occurred at the projectile-target interfaces, Figure 13. During examination of the ballistic craters deposits were observed on the interface. EDX-spectroscopy of the deposits showed a significant concentration of iron. Because of the negligible iron content of the titanium alloy it is assumed that the iron was transferred from the projectile. (Appendix, Diagram 1 to 3)
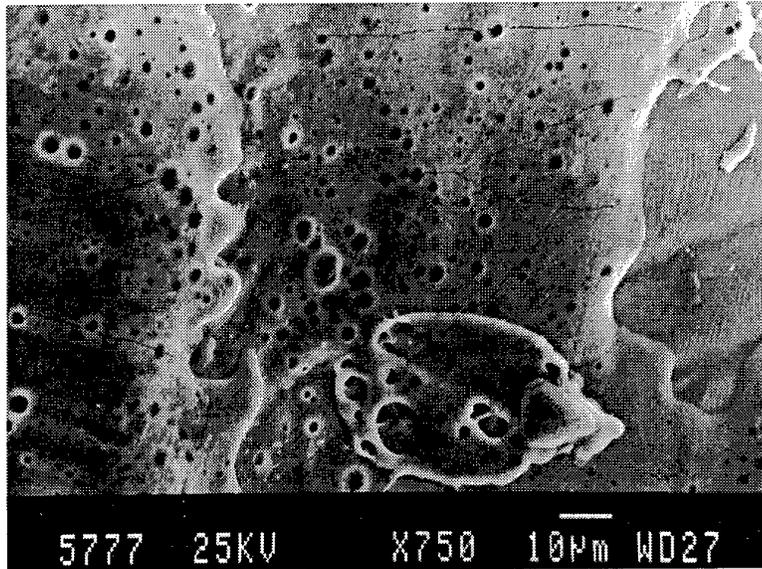
Figure 13: Melted parts of the surface of the ballistic crater, 67 186, VCF, 899 °C - 30 min - AC, SEM 5777

During sectioning, ballistic craters of 67 190 and 67 186 were broken into pieces at sheared and/or spalled planes. The spalled parts and surfaces were investigated using SEM.
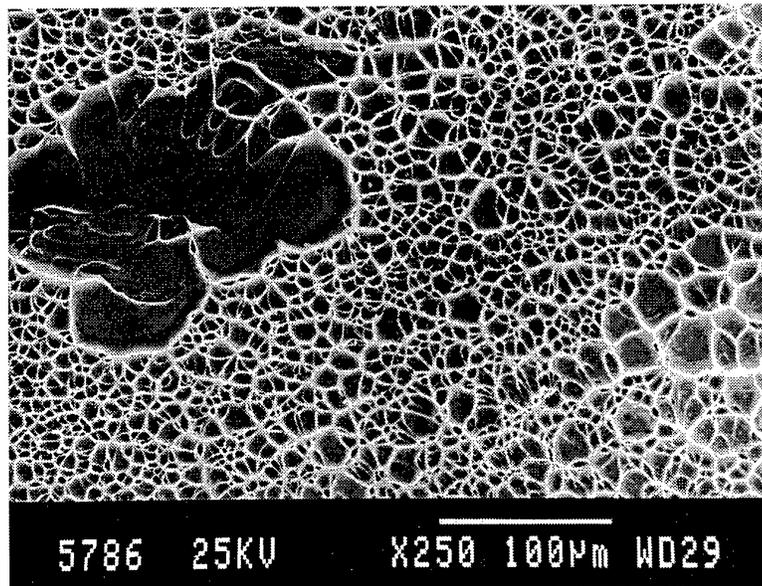
Figure 14: Sheared and fractured/spalled surface inside of the cracked ballistic crater, 67 190, VCF only, SEM 5786

Cavities are present in the shear band of the ballistic as well as laboratory samples, Figure 14 to Figure 16. In shear cracks of the ballistic crater and on the surface of compression/shear specimens, fracture surfaces exhibit relatively smooth surfaces, which contain many dimples that are characteristic for ductile fracture.
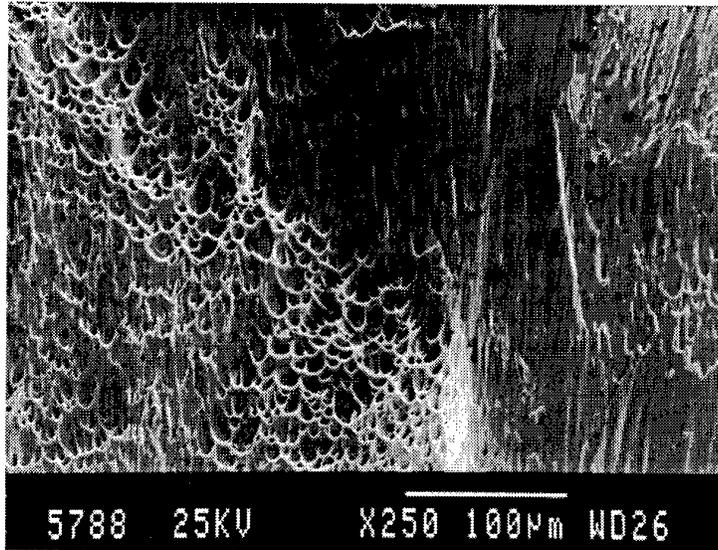
Figure 15: Surface inside of the sheared and cracked ballistic crater, 67 190, VCF only, SEM 5788
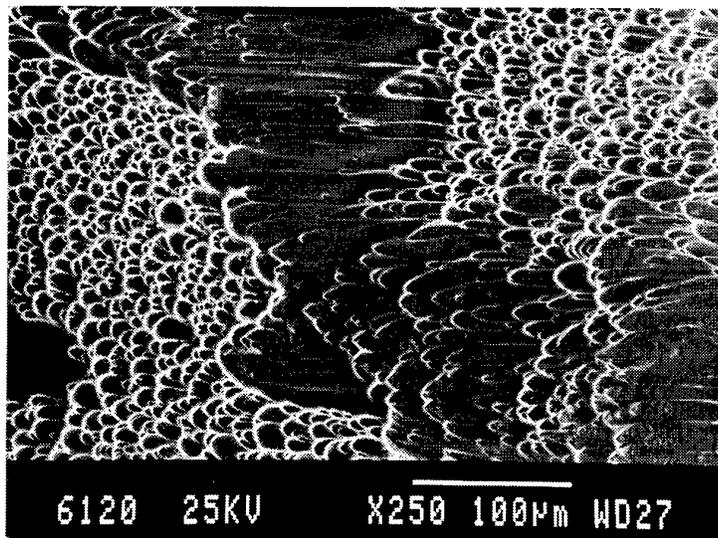
Figure 16: Surface of compression/shear specimen, 184-4-42, 6 °, VCF, 1038 °C-30 min-AC, SEM 6120

Observations of the failure of dynamically loaded specimens are consistent with the mode of adiabatic shear bands which are formed in ballistic craters. Investigations of fractured surfaces of laboratory specimens and ballistic samples have shown both, smooth surfaces and in some sites surfaces with cavities and dimples. This is a characteristic of a ductile fracture. The occurrence of cracks and voids inside the shear bands in ballistic craters and the observations on the spalled/sheared places let assume, that there must be additionally tensile stresses as reported in [21]. They are a result of wave propagation and reflection during impact loading. Furthermore, thermal effects, i.e. the dilatation gradient, can induce tensile stress states too [22].

3.3   INTERDEPENDENCIES BETWEEN MECHANICAL AND BALLISTIC DATA

Ballistic tests have shown, that the annealing conditions could have strong influence on ballistic performance. Annealing above the beta transus temperature leads to a loss in the normalized V_{50} limit velocity, Figure 17.
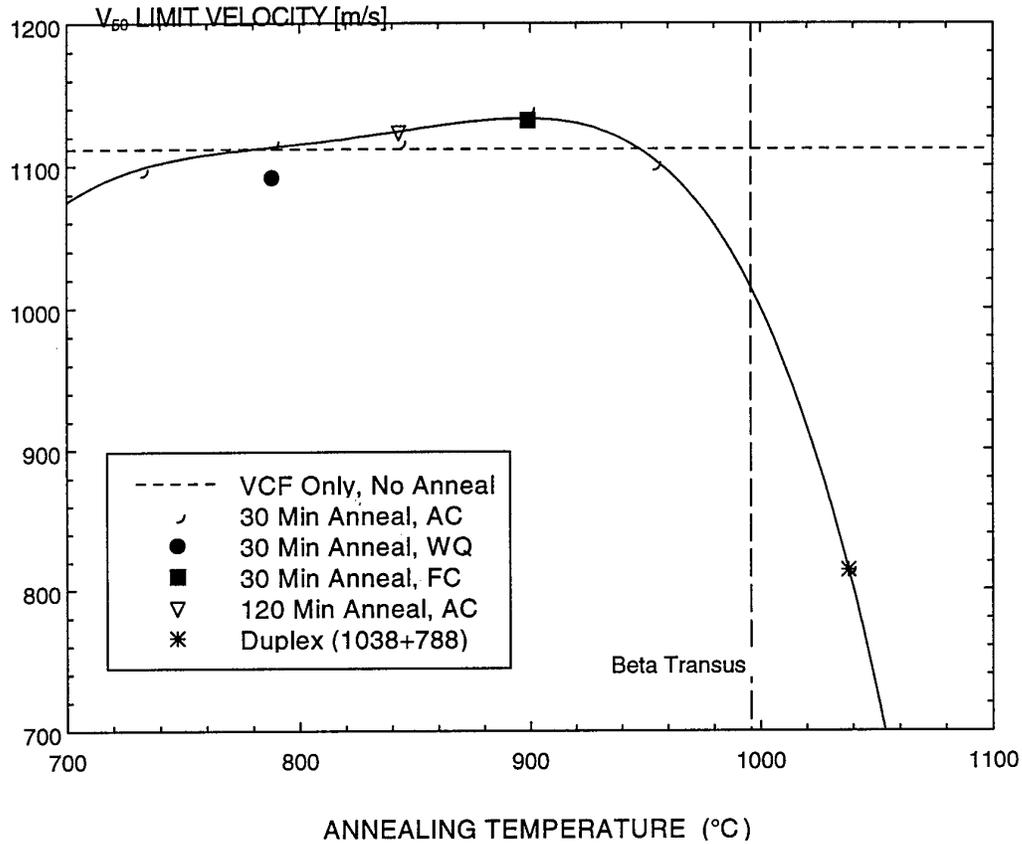
Figure 17: Normalized V_{50} limit velocity as a function of annealing temperature, [23]

Some indications of interdependencies between the ballistic performance of different heat treated titanium targets were noted, especially, the dynamic strength and sensitivity to adiabatic shear failure under dynamic biaxial conditions. As shown in Figure 18, when the ballistic performance decreases, the failure strain, the compressive plastic deformation of the occurrence of adiabatic shear failure, is reduced too. Therefore, the incidence of failure seems to correlate with the ballistic performance of these alloys.
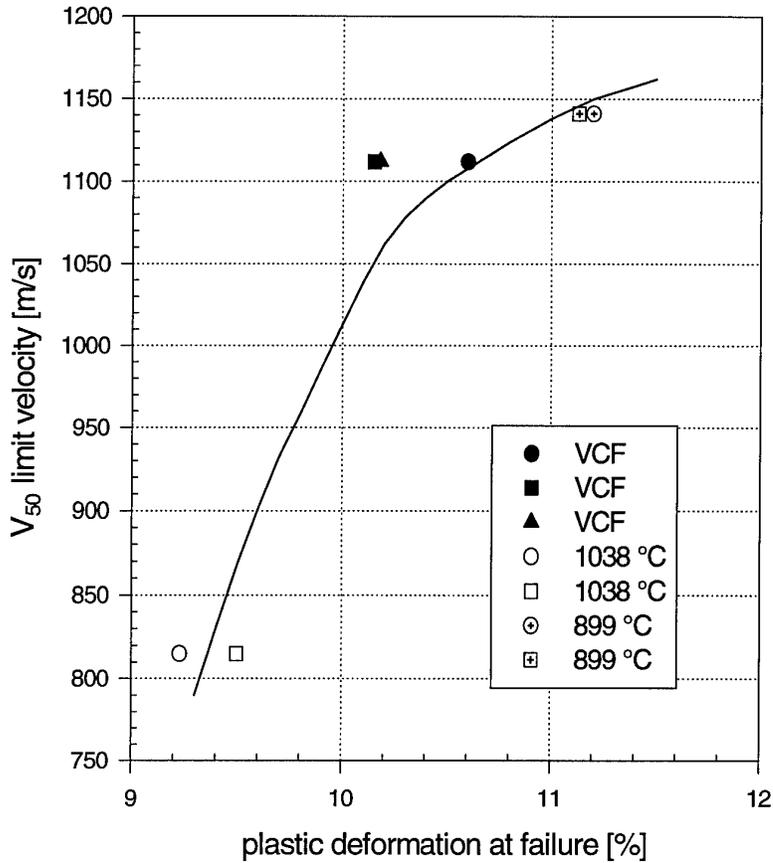
Figure 18: Plastic deformation at failure under dynamic shear/compression loading
(specimen inclination 10 °; τ/σ=17,63, $\dot{\varepsilon}$ = 200 s^{-1})

Furthermore, the influence of heat treatment on the energy consumption during dynamic compression/shear tests was investigated, Figure 19. The energy consumption of the compression/shear process is given by the integral of the force/displacement curve. Annealing over the beta transus temperature reduces the work of deformation, which correlates with the limit velocity.
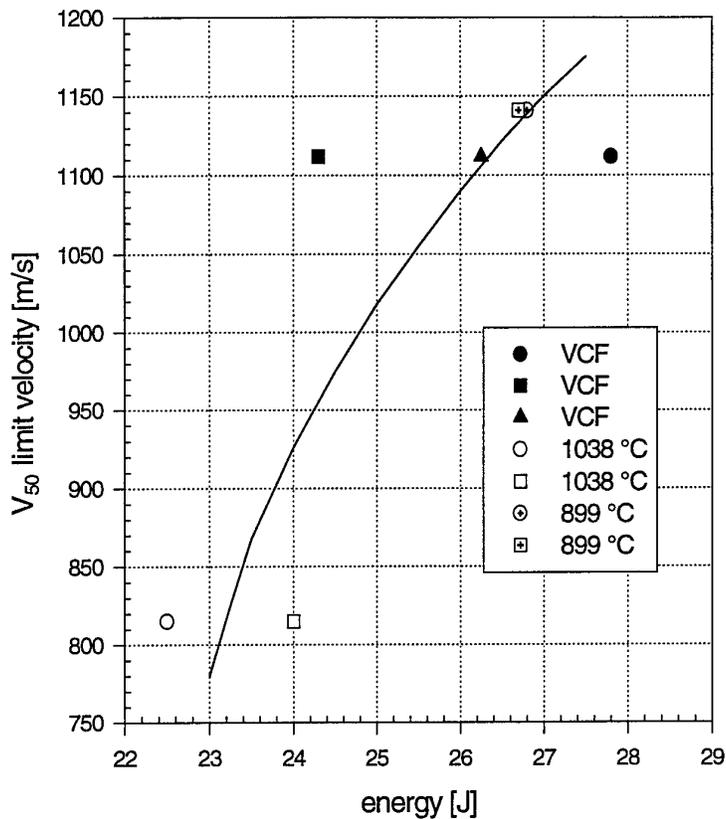
Figure 19: Absorbed energy under dynamic shear/compression loading
(specimen inclination 10 °; τ/σ=17,63, $\dot{\varepsilon} = 200 \text{ s}^{-1}$)

4   CONCLUSION

Ballistic and mechanical tests were performed on Ti-6Al-4V subjected to three different heat treatments. Some indications of interdependencies between the ballistic performance of different heat treated titanium targets were noted, especially, the dynamic strength and sensitivity to adiabatic shear failure under dynamic biaxial conditions. The characteristic values obtained from dynamic shear/compression tests such as the engineering compressive strength, the strain up to failure and the absorbed energy are suitable to find interdependencies to the ballistic performance.

5   ACKNOWLEDGEMENTS

6   LITERATURE

[1]   Boyer, R., R.: An overview on the use of titanium in the aerospace industry; Materials Science and Engineering A213 (1996) 103-114

[2]   Gooch, M. S. Burkins, H.-J. Ernst and T. Wolf, „Ballistic Performance of Titanium against Laboratory Penetrators with Aspect-Ratios of 10 or Greater, Proceedings of the 15th International, Ballistics Symposium, Jerusalem, Israel, 1995

[3]   W. Gooch, M. S. Burkins, H.-J. Ernst and T. Wolf: Ballistic Penetration of Titanium Alloy Ti-6Al-4V, Proceedings of the Lightweight Armour Systems Symposium, The Royal Military College of Science, Shrivenham, Swindon, England, 1995

[4]   W. Gooch, M. Burkins and K. Frank: Ballistic Performance of Titanium against Laboratory Penetrators, Proceedings of the 1st Australasian Congress on Applied Mechanics, Melbourne, Australia, 21-23 February 1996

[5]   S. Bless et al.: Penetration Resistance of Titanium and Ultra-hard Steel at Elevated Velocities, Proceedings of the 1996 Hypervelocity Impact Society Symposium, Freiburg, Germany, 7-10 October 1996

[6]   M. Burkins and J. Paige: A Ballistic Evaluation of Ti-6Al-4V versus Long-rod Penetrators, ARL-TR-1146, July 1996

[7]   Meyer, L., W., Krueger, L., Chaiat, D., Weinberger, C., Rosenberg, Z.: Correlation between ballistic and material behavior under high strain rates; ISIE, Peking, 1996

[8]   Giovanola, J. H.: Observation of adiabatic shear banding in simple torsion, Impact Loading and Dynamic Behaviour of Materials, eds C. Y. Chiem, H.-D. Kunze and L. W. Meyer, DGM-Verlag, Oberursel, Germany, pp. 705-710, 1988

[9]   Bai, Y., Xue, Q., Xu, Y., Shen, L.: Characterisation and microstructure in the evolution of shear localisation in Ti-6Al-4V alloy; Mechanics of Materials 17 (1994) pp. 155-164

[10]   Meyer, L. W., Manwaring, S.: Critical adiabatic shear strength of low alloyed steel under compressive loading, Metallurgical Applications of Shock-Wave and High-Strain-Rate Phenomena, Marcel Dekker, ed. by L. E. Murr, K. P. Staudhammer and M. A. Meyers, 1986, pp. 657-673

[11]   Meyers, M. A., Subash, G., Kad, B. K., Prasad, L.: Evolution of microstructure and shear-band formation in α-hcp titanium, Mechanics of Materials 17 (1994) pp. 175-193

[12]   Grebe, H. A., Pak, H.-R., Meyers, M. A.: Adiabatic Shear Localisation in Titanium and Ti-6 Pct Al-4 Pct V Alloy; Metallurgical Transaction A, Vol. 16A, May 1985, 761-775

[13]   Bai, Y., Xue, Q., Xu, Y., Shen, L.: Macroscopic scaling and microstructural evolution in shear band phenomena, Metallurgical and Materials Applications of Shock-Wave and High-Strain-Rate Phenomena (EXPLOMET'95), 1995, pp. 377-388

[14]   Dinzart, F. and Fressengeas, C.: Shear band with in thermo-viscoplastic heat-conducting materials; Metallurgical and Materials Applications of Shock-Waves and High-Strain-Rate Phenomena, (EXPLOMET'95), ed. by L. E. Murr, K. P. Staudhammer and M. A. Meyers, 1995, Elsevier, pp.405-411

[15]   Nemat-Nasser, S. et al.: Experimental/computational evaluation of flow stress at high strain rates with application to adiabatic shear banding, Mechanics of Materials 17 (1994), pp. 111-134, Elsevier

[16]   Wood, J. R.: Evaluation of Ballistically Tested Ti-6Al-4V ELI Armor Plate in Various Annealed Conditions; Technical Memo 96-16, RMI Titanium Company, 1996

[17]   Meyer, L. W.: Adiabatic shear failure under dynamic biaxial compression shear loading, EUROMECH 282 Symposium, Presentation, Metz, France, 8-11 July 1991

[18]   Meyer, L. W., Staskewitsch, E. and A. Burblies: Adiabatic shear failure under biaxial dynamic compression/shear loading, Mechanics of Materials 17, 1994, pp. 203-214

[19]   Meyer, L. W.: Conditions of Adiabatic Shear in Dynamic Torsional and Compressive Loading of Ti-Al6-V4 Titanium Alloy, Titanium, Science and Technology, ed. by Lütjering, Zwicker, U. and Bunk W., DGM, 1984, pp. 1851-1858

[20]   Follansbee, P. S. and Gray, G. T. III.: An Analysis of the Low Temperature, Low and High Strain-Rate Deformation of Ti-6Al-4V, Metallurgical Transaction A, Vol. 20A, May 1989, pp. 863-874

[21]   Rogers, H. C.: Material Behviour under High Stress and Ultra High Loading Rates, 1983, ed. by J. Mescall and V. Weiss, Plenum Press NY, USA, pp. 101-118

[22]   Dormeval, R.: Adiabatic Shear Phenomena, Impact Loading and Dynamic Behaviour of Materials, ed by C. Y. Chiem, H.-D. Kunze and L. W. Meyer, DGM Informationsgesellschaft mbH, 1988, pp. 43-56

[23]   Burkins, M.; Love, W.: Effect of Annealing Temperature on the Ballistic Limit Velocity of Ti-6Al-4V ELI, 16th International Symposium on Ballistics, San Francisco, 1996, pp. 723-732

7 APPENDIX

7.1 TABLES

Table 3: Results of hardness measurements HV 10 on the received plates

	Direction of Measurement	Mean	Minimum	Maximum	Standard Deviation
67 190	thickness	289	272	309	9,5
67 190	thickness	287	266	306	9,7
67 184	thickness	317	281	360	22,06
67 184	thickness	313	285	387	25,29
67 186	thickness	285	262	317	12,39
67 186	thickness	284	266	306	9,07
67 190	opposite to rolling dir.	289	274	317	11,58
67 190	opposite to rolling dir.	291	272	342	17,38
67 184	opposite to rolling dir.	313	290	357	17,14
67 184	opposite to rolling dir.	304	276	342	17,75
67 186	opposite to rolling dir.	286	272	299	7,7
67 186	opposite to rolling dir.	279	268	299	6,4
67 190	in rolling direction	295	279	311	10,28
67 190	in rolling direction	299	287	314	9,02
67 184	in rolling direction	352	322	383	18,6
67 184	in rolling direction	352	330	387	16,2
67 186	in rolling direction	294	279	330	12,4
67 186	in rolling direction	302	290	317	8,2

Table 4: Microhardness measurement in the coarse grained material, force: 10 p,
specimen: 360, 67184, VCF, 1038 °C - 30 min - AC

Microhardness in the bright grain boundaries	Microhardness in the grains
368	339
389	339
401	339
321	321
321	321
378	339
321	348
368	339
mean: 358	mean: 336

7.2 DIAGRAMS
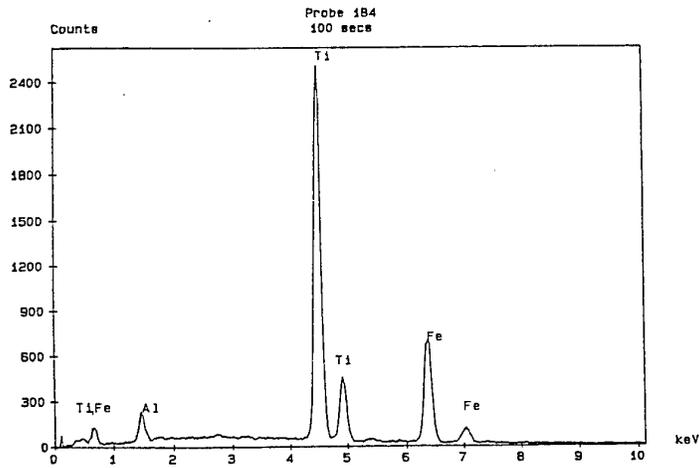
Diagram 1: EDXS - profile on the surface of the ballistic crater, 67 184
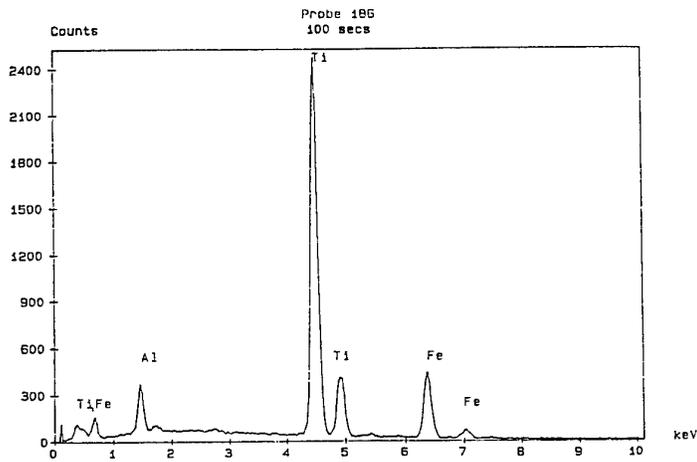
Diagram 2: EDXS - profile on the surface of the ballistic crater, 67 186
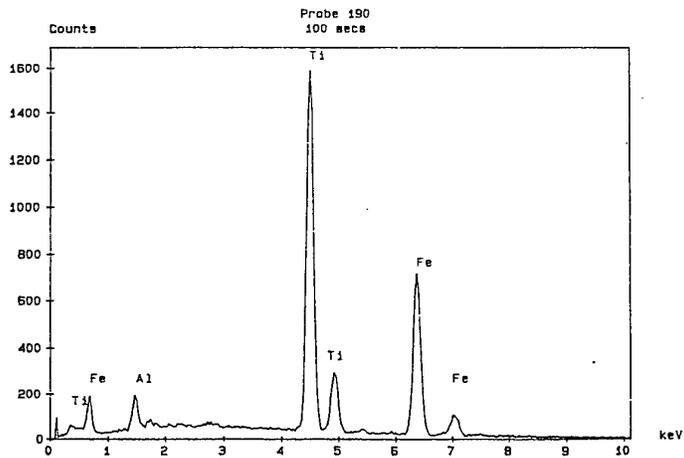
Diagram 3: EDXS - profile on the surface of the ballistic crater, 67 190